Estimation of k L a values in a Bench-Scale Stirred Tank Reactor Equipped with a Self-Inducing Impeller

Vania Santos-Moreau, José Carlos B. Lopes, Cláudio P Fonte

Estimation of k_La values in a Bench-Scale Stirred Tank Reactor Equipped with a Self-Inducing Impeller

Vania Santos-Moreau[1], José Carlos B. Lopes[2], Cláudio P. Fonte[3**]*

1 – IFP Energies Nouvelles, Rond-point de l'échangeur de Solaize - BP 3, 69360 Solaize, France

2 – LA LSRE/LCM, Laboratory of Separation and Reaction Engineering, Faculdade de Engenharia, Universidade do Porto, Rua Dr. Roberto Frias s/n, 4200-465 Porto, Portugal

3 – School of Chemical Engineering and Analytical Science, The University of Manchester, Oxford Road, Manchester, M13 9PL, United Kingdom

* email: vania.santos@ifpen.fr

** email: claudio.fonte@manchester.ac.uk

Abstract

A multiphase CFD simulation methodology has been developed and proposed for the estimation of the spatial distribution of k_La values in a bench-scale reactor equipped with a self-inducing impeller. The importance of estimating an apparent drag coefficient that considers the effect of turbulence on the gas bubbles rising velocity is also tackled in this work. This has been done by using different correlations available in the literature: the Brucato, the Modified Brucato and the Pinelli correlation. The spatial distribution of k_La values in the agitated vessel has been obtained from the CFD results using Danckwert's surface renewal model. An analysis of the gas volume fraction distribution obtained from the simulations has been performed in order to choose the most suitable drag model. The modified Brucato correction correlation for the drag force shows the best agreement with experimental data.

Keywords

Multiphase reactor; CFD model; Stirred tanks; Mass transfer; Gas dispersion

1 Introduction

Different technologies to promote the dispersion of the gas into the liquid, such as spargers, gas ejectors and self-inducing impellers, are used from the laboratorial to the industrial scale. Self-inducing impellers have hollow shafts that draw gas captured from above the free-surface down into the liquid, without the need for additional devices. Simultaneously, the flow turbine of the self-inducing impeller promotes the dispersion and mixing of the gas in the agitated liquid. Its operation principle is based on the pressure gradient generated due to rotation between inlet orifices at the top of the shaft (above the liquid level) and orifices placed near the impeller blades (immersed in the agitated liquid). The pressure gradient generated between the two orifices, for sufficiently high impeller speeds (the critical speed), promotes a continuous suction of gas at the top that flows through the hollow shaft and is released into the liquid. Further details on the gas-induction mechanisms can be found in [3,4]. If the reactor is operated in batch mode, the gas that is not absorbed into the liquid escapes from the free surface to be re-circulated again. This makes self-inducing impellers an attractive solution when the recycling gas is costly, not abundant, or hazardous.

In the turbulent regime, the gas-liquid mass transfer rate is directly related to the amount of interfacial area generated between the two phases and local values of turbulence dissipation in the flow. These values depend simultaneously on the impeller geometry and dimension, its rotational speed, and on the physical properties of the fluids. Understanding the phenomena taking place and studying the effect of different reactor designs and operating conditions on the critical impeller speed for gas suction, gas suction rate, gas holdup, gas/liquid mass transfer, power consumption, etc., is thus essential for controlling its operation. Several authors have been studying experimentally and through numerical modeling these kind of systems for different applications, both gas-liquid or gas-solid-liquid [5–15].

This study focus on a bench-scale stirred reactors equipped with hollow self-inducing impellers that are used to mimic industrial processes of the Oil and Gas industry. A good replication of the hydrodynamic and mass transfer rate conditions allows to test industrial processes at a smaller scale, reducing costs associated to construction and operation. It is known, nonetheless, that gas/liquid mass transfer rates depend on the size of the vessel, blending time, induced gas flow rate, power dissipation rate, etc., and do not scale all in the same manner with size. Industrial-size reactors are more limited than bench-scale reactors [16] : typical industrial mass transfer coefficients, $k_L a$, have often values around $0.1\ s^{-1}$, rarely exceeding $0.3\ s^{-1}$; whereas in bench-scale stirred reactors the $k_L a$ can be higher than $1\ s^{-1}$ [12]. For this reason, multiphase stirred tank reactors equipped with self-inducing impellers are difficult to scale since complex coupled phenomena take place. In order to obtain a bench-scale reactor that is representative of the industrial unit, it is important to know how to adequate the bench-scale operational conditions to the range of $k_L a$ values found during the industrial operation.

To obtain $k_L a$ values in bench-scale stirred reactors, mass transfer experiments should be performed since the majority of existing correlations in the scientific literature cannot be used. Usually, these correlations were developed for industrial-sized reactors and are based on values of power dissipation, gas flow rate and gas holdup. At the bench-scale these quantities are not easily determined experimentally. Power dissipation from direct electrical measurements must be done with extreme care at the bench-scale since friction losses can represent up to 70% of the total power and need to be quantified. More accurate techniques are required to overcome this issue, such as dynamometers or torque meters, but substantially bigger investment is necessary [17]. Different authors developed experimental methodologies to determine $k_L a$ following the physical absorption of the gas [2,18–20]. This method is

simple to set up since most bench-scale units are equipped with pressure sensors. Some authors have applied those methods to the characterization of bench-scale reactors [2,12,20–24].

Alternatively, $k_L a$ values can be estimated from Computational Fluid Dynamics (CFD) simulations. Several authors such as Buffo et al. [25] and Gimbun et al. [26] have previously used this approach to estimate the spatial distribution of the gas in the agitated liquid and the interfacial mass transfer rate in medium-sized and large scale reactors. The multiphase flow inside the vessel was simulated following an Euler-Euler modeling approach, and $k_L$values have been estimated from the flow simulations using Danckwerts' surface renewal model [1]. To take into account the bubbles coalescence and breakup, these authors have proposed the use of Population Balance Models (PBM). The use of PBM increases considerably the CFD model complexity and requires experimental data of coalescence and break-up rates to be included in the model. When breakup and coalescence are not the most significant phenomena, the CFD model can be considerably simplified assuming spherical-shaped bubbles with a mono-dispersed size. Many modelling studies on gas-liquid stirred tanks have been performed in recent years, using a uniform mono-dispersed bubble size giving satisfactory results in terms of gas holdup and mean flow [27–32].

The objective of this work is the development of a computational model for the prediction of gas-liquid mass transfer rates in a bench-scale stirred reactor equipped with a self-inducing impeller. To be able to be used as an optimisation tool, this computational model should be as inexpensive as possible on what hardware requirements and simulation time are concerned. The flow was simulated using an Euler-Euler multiphase modelling, considering a mono-dispersed bubble size throughout the tank. The results will allow adapting the bench-scale reactor operational conditions to industrial G/L mass transfer performances. In addition, the

CFD simulations provide spatial distributions of $k_L a$ in the reactor that allow identifying zones of poor mass transfer rate.

2 Studied reactor geometry

The studied device is a batch bench-scale cylindrical flat-bottomed reactor from *Top Industrie* with a diameter of 58 mm and a total volume of 300 cm^3 (Figure 1, left). Gas suction and mixing are promoted by a stainless steel radial flow self-inducing impeller with a diameter of 19 mm (Figure 1, right) from *Top Industrie*. The main difference between a standard Rushton turbine and the used impeller resides in the fact that the blades in the latter are welded to two disks instead of one. The two disks help the mechanical conception of this small hollow. In addition, the ratio between the blade height and the impeller diameter is considerably different for the two geometries: this ratio is usually 0.20 to 0.25 for Rushton turbines and 0.52 for this self-inducing impeller. Four equally spaced baffles with a length of 10 mm are placed in the reactor to avoid the formation of a free-surface vortex due to the impeller rotation. To help the mechanical conception of the baffles of this small reactor a B/T=0.17 was chosen.

In order to promote gas suction, two inlets are located at the top of the hollow shaft, above the liquid free surface, and six outlets are located in the middle of the impeller, between each pair of blades and between the disks. The internal diameter of the hollow shaft is equal to 3 mm and the inlet and outlet orifices have a diameter equal to 1.5 mm. Figure 2 shows a schematic representation with the main dimensions of the bench-scale reactor and the self-inducing impeller.

The multiphase system considered in this work was a mixture of methylcyclohaxane/hydrogen at 10 bar and 20 °C. The reactor is filled with methylcyclohexane, until a height of 50 mm from the bottom.

3 Numerical simulations

3D steady state two phase CFD simulations have been performed to obtain the flow field of the liquid and the gas in the stirred tank. Details on the development of the flow model and the adopted numerical methodologies for the flow simulations are described here.

3.1 Two-fluid Euler-Euler flow modelling

A two-fluid Euler-Euler approach was used in the development of the flow model of the agitated gas-liquid mixture in reactor. This approach describes the motion for each phase in a macroscopic but space-resolved sense, considering the two fluids as two interpenetrating continua. Mass and momentum conservation equations are solved for each of the two phases individually considering interaction terms between them. In steady state, mass conservation for each phase $i = \{G, L\}$ is mathematically described by

$$\nabla \cdot \left(\alpha_i \rho_i \vec{u}_i \right) = \nabla \cdot \left(\Gamma_i \rho_i \nabla \alpha_i \right), \tag{1}$$

where α_i the volume fraction, ρ_i the density, $\vec{u}_i$ the velocity field of phase i in the flow. For simplicity, the bubble path dispersion has been chosen to be modelled as a diffusive term with a dispersion coefficient Γ_i rather than baing treated as an interfacial momentum force in the momentum conservation equations. Further details on this simplified but established approach for modelling turbulence-induced bubble dispersion can be found in [33]. The dispersion coefficient for the gas phase, Γ_G, can be estimated from the turbulent viscosity in the liquid phase, $\nu_{T,L}$, as

$$\Gamma_G = \frac{\nu_{T,L}}{\mathrm{Sc}_{T,\mathrm{VOF}}} \tag{2}$$

where $\mathrm{Sc}_{T,\mathrm{VOF}}$ is the turbulent Schmidt number for the phases. A default value of 0.75 for $\mathrm{Sc}_{T,\mathrm{VOF}}$ has been considered in the simulations. In order to retain global continuity in the system, the dispersion term of Equation (1) for the liquid phase must be equal to

$$\nabla\cdot\left(\Gamma_L\rho_L\nabla\alpha_L\right)=-\nabla\cdot\left(\Gamma_G\rho_G\nabla\alpha_G\right). \tag{3}$$

The momentum conservation equations for each phase are coupled through the domain pressure (shared by both phases) and interphase momentum exchange coefficients. The momentum conservation equation for each phase $i=\{G,L\}$ are

$$\nabla\cdot\left(\alpha_i\rho_i\vec{u}_i\vec{u}_i\right)=-\alpha_i\nabla p+\nabla\cdot\bar{\bar{\tau}}_i+\alpha_i\rho_i\vec{g}+\vec{F}_{Drag,i}+\vec{F}_{Non-drag,i} \tag{4}$$

where p the pressure field in the vessel and $\vec{g}$ the gravity acceleration. $\vec{F}_{Drag,i}$ is the drag force of the gas bubbles, and $\vec{F}_{Non-drag,i}$ are other interaction forces such as lift, virtual mass forces and turbulent dispersion forces. The stress tensor, $\bar{\bar{\tau}}_i$, for the phase i is given by

$$\bar{\bar{\tau}}_i=\alpha_i\mu_i\left(\nabla\vec{u}_i+\nabla\vec{u}_i^{\mathrm{T}}\right)+\alpha_i\left(\lambda_i-\frac{2}{3}\mu_i\right)\left(\nabla\cdot\vec{u}_i\right)\bar{\bar{I}} \tag{5}$$

where μ_i is the dynamic viscosity, λ_i is the bulk viscosity and $\bar{\bar{I}}$ is the identity tensor. Gravity was set to act on the system vertically, i.e., along the impeller axis, and downwards. The drag force on the moving bubbles was the only considered momentum exchange term between the two phases. Other contributions to the exchange of momentum between phases, like lift and virtual mass forces, have been reported in the literature to be non-dominant in multiphase stirred vessels [31], and therefore have not been considered in the model. The drag force was calculated as

$$\vec{F}_{Drag,L}=-\vec{F}_{Drag,G}=C_D\frac{3}{4}\rho_L\frac{\alpha_G}{d_b}\left|\vec{u}_G-\vec{u}_L\right|\left(\vec{u}_G-\vec{u}_L\right) \tag{6}$$

where C_D is the drag coefficient and d_b the bubbles mean diameter.

The turbulent properties of the flow in the stirred tank were simulated by solving the Reynolds-Averaged form of the Navier-Stokes (RANS) equations. This solution method was used since it requires less computational power than more advanced methods such as LES modelling or DNS. While not providing the most detailed description of all flow scales, RANS turbulence modelling is more attractive and practical in an industrial application context due to their lower computational requirements. The turbulence in the flow was simulated with the Multiphase Realizable *k-ε* Model with standard wall functions for each phase, which solves a set of turbulent kinetic energy and turbulent energy dissipation rate transport equations for each of the two fluids [34]. Previous works have shown that this is the most suitable turbulence model for the simulation of the flow in this device [45]. The $k-\varepsilon$ model constants C_2, C_3, σ_k, σ_ε, σ_{GL} were set with default values of 1.9, 1.3, 1, 1.2, 0.75, respectively.

3.2 Drag coefficient estimation in mechanically induced turbulence

The bubble drag coefficient was calculated from the Schiller-Naumman [35] and Tomiyama [36] correlations. From the Schiller-Naumann correlation, C_D is estimated by

$$C_D = \begin{cases} \dfrac{24}{\mathrm{Re}}\left(1+0.15\,\mathrm{Re}^{0.687}\right) & \text{if } \mathrm{Re} \le 1000 \\ 0.44 & \text{if } \mathrm{Re} > 1000 \end{cases}, \tag{7}$$

where Re is the bubble Reynolds number

$$\mathrm{Re} = \frac{\rho_L \left|\vec{u}_G - \vec{u}_L\right| d_b}{\mu_L}. \tag{8}$$

The Schiller-Naumann correlation is well suited to flows regimes with non-deformed spherical bubbles. For flow regimes where the bubbles present non-negligible shape deformation (ellipsoids or spherical caps), the Tomiyama correlation has been proposed. In this empirical model, C_D is estimated by

$$C_D = \max\left(\min\left(\frac{24}{\mathrm{Re}}\left(1+0.15\,\mathrm{Re}^{0.687}\right), \frac{74}{\mathrm{Re}} \right), \frac{8}{3}\frac{\mathrm{Eö}}{\mathrm{Eö}+4} \right) \tag{9}$$

where Eö is the Eötvös number, the ratio between the buoyancy forces and surface tension forces, given by

$$\mathrm{Eö} = \frac{g\left(\rho_L - \rho_G\right) d_b^2}{\sigma}, \tag{10}$$

where σ is the surface tension.

These two drag models have been tested at the same operational conditions (1600 rpm, bubble mean diameter of 2 mm, same fluids, etc.). No significant differenced has been observed in the estimated value of $k_L a$ and in the gas distribution in the tank and, for that, reason the Schiller-Naumann correlation was chosen to proceed the calculations. This choice is also supported by flow visualizations in a transparent reactor, which show mainly non-deformed spherical bubbles. While Equations (7) and (9) can predict quite well the drag coefficient of individual bubbles in quiescent flows, they may produce large errors under mechanically-generated turbulence or non-stationary conditions. Free-stream velocity fluctuations have been reported from experiments to decrease substantially the settling velocity of solid particles, in some cases to as low as 15% of the value in a quiescent liquid [37]. This decrease on the settling velocities of solid particles or rising velocities of bubbles may be explained by constant accelerations and decelerations of the particles or bubbles in the flow due to turbulent/stochastic velocity fluctuations. Added mass forces acting on the particle due to the accelerations and decelerations, and the fluctuations in the instantaneous value of the drag coefficient combined with its non-linear dependence with the velocity may appear as an increased time-averaged drag coefficient. Brucato el al. [37] proposed an empirical-based correlation obtained from experimental measurements of the settling velocity of solid particles in a Taylor-Couette flow

$$\overline{C_D} = C_D\left(1+8.7\times10^{-4}\left(\frac{d_b}{\lambda_K}\right)^3\right) \tag{11}$$

where $\overline{C_D}$ is the apparent drag coefficient under turbulent conditions and C_D the drag coefficient of a single bubble in quiescent conditions. This correction is a function of the ratio between the diameter of the bubbles and the Kolmogorov scale,

$$\lambda_K = \left(\frac{\nu_L^3}{\varepsilon_L}\right)^{1/4}, \tag{12}$$

for the estimation of a corrective term for the drag coefficient. It can be argued that, since Equation (11) has been obtained for solid particles, it must be assumed that mechanisms of drag modification due to free-stream turbulence are the same for solid particles and gas bubbles. It is to expect that the difference between the density of the liquid and the gas bubbles or solid particles on settling/rising velocities should be taken into consideration as more recently pointed out by Doroodchi et al. [38].

Later, Lane et al. [39] propose a modification to Brucato's correlation constant

$$\overline{C_D} = C_D\left(1+6.5\times10^{-6}\left(\frac{d_b}{\lambda_K}\right)^3\right) \tag{13}$$

This modification was found to offer better results on a simulation of the gas distribution and holdup in stirred tank reactor, which allows to infer as well that the density difference between the liquid and the inclusions has a relevant impact on drag modification due to turbulence. However, and notwithstanding the better results that have been obtained, the proposed modification is still lacking more solid physical grounding. More recently, Pinelli et al. [40] proposed a correlation for the particle settling in stirred vessels that also takes into account the ratio d_b / λ_K

$$\overline{C_D} = C_D\left(0.4\tanh\left(16\frac{\lambda_K}{d_b}-1\right)+0.6\right)^{-2} \tag{14}$$

obtaining good results on the modeling the dispersion and sedimentation of particles in baffled and unbaffled stirred tank reactors with multiple impellers.

3.3 Gas-liquid mass transfer rate estimation

The spatial distribution of the gas-liquid mass transfer rate, $k_L a$, in the stirred reactor was obtained from the CFD simulations using Danckwerts' surface renewal model [1]. Danckwerts proposed that the mass transfer rate between the two phases could be related to an average surface renewal rate, which is resulting from the contact of the bubbles' interface with the turbulent eddies in the liquid phase as

$$k_L = \sqrt{D_m s} \tag{15}$$

where s is the rate of renewal liquid at the surface of the gas bubbles and D_m the diffusivity of the absorbed gas in the liquid. Lamont and Scott [41] developed Danckwerts' assumption further based on the statistical theory of turbulent diffusion by assuming s to be inversely proportional to the Kolmogorov time scale, $s \propto \tau_\eta^{-1} = \left(\nu_L / \varepsilon_L\right)^{-1/2}$. The gas/liquid coefficient k_L can then be estimated by

$$k_L = C\sqrt{D_m}\left(\frac{\varepsilon_L}{\nu_L}\right)^{1/4} \tag{16}$$

where C is the model constant equal to 0.4. The specific surface area of the bubbles, a, was obtained considering the *Symmetric* model, which ensures that the specific area approaches the value 0 as the volume fraction of gas approaches the value 1,

$$a = \frac{6}{d_b}\alpha_G\left(1-\alpha_G\right) \tag{17}$$

The molecular diffusivity of hydrogen in methylcyclohexane was estimated with the Wilke-Chang correlation for the conditions of the experiments [42].

3.3.Mesh, boundary conditions and numerical methods

The geometrical domain and numerical grid for the flow simulations were generated with the software packages *DesignModeler* and *Meshing*, respectively, included in the ANSYS 15 suite. All the internal parts of the reactor were generated with the same geometric dimensions as the ones of the existing setup, with the exception of the thickness of the impeller and baffles which have been neglected. Recent computational studies have shown that accurate velocity profiles can be obtained computationally even when the thickness of impeller blades, impeller disk and baffles is neglected [43].

The geometrical domain of the entire stirred tank was discretized with a computational conformal and structured mesh obtained from 600 k hexahedral elements with typical sizes ranging from 0.2 to 0.6 mm (Figure 3 and Figure 4). Beyond this number of elements, the numerical results of velocity and turbulence quantities have been observed to be independent from the mesh refinement. The mesh has a higher element density in the impeller zone, where higher spatial gradients are expected. The necessary higher values for the mesh density at the walls were established by ensuring that the distance of the first volume element from any wall of the reactor, in terms of the dimensionless distance, y^+, are smaller than 300 and mostly comprised between $30 \leq y^+ \leq 300$.

The boundary conditions were set as follows. No-slip and impermeable conditions at the vessel walls have been assumed for both phases. The top surface of the vessel was set as a non-deformable surface with constant and uniform pressure equal to the atmospheric pressure (pressure outlet). Through this surface, both the gas bubbles and the liquid were allowed to leave the domain, however only liquid was allowed to re-enter. This approach, although not

completely satisfying in a physical sense, has been reported in previous works to be a good compromise between accuracy and ease of solution [25,44]. The gas phase was set to enter the domain from the surfaces representing the impeller orifices immersed in the liquid. The gas inlet velocity was set to be normal to the inlet surfaces, with a magnitude depending on the impeller rotational velocity. The relation between the impeller rotation speed, *N*, in rpm and the induced gas flow rate into the liquid, Q_G, in m^3/s for the devide of this study has been reported in the literature as [45]

$$\log_{10} Q_G = \begin{cases} 1 & \text{if } \Delta p_{imp} \le 0 \\ b_1 \left(\log_{10} \Delta p_{imp} \right)^2 + b_2 \left(\log_{10} \Delta p_{imp} \right) + b_3 & \text{if } \Delta p_{imp} > 0 \end{cases} \tag{18}$$

where Δp_{imp} is the pressure drop due to friction in the impeller shaft, in Pa, and for $b_1 = -0.0645$, $b_2 = 0.945$, and $b_3 = -6.1$. Δp_{imp} can estimated from

$$\Delta p_{imp} = a_1 N^{a_2} - \frac{2\sigma}{d_o} \tag{19}$$

where σ is the surface tension, d_o is the self-inducing impeller orifices diameter, and the constants have values $a_1 = 0.0721$ and $a_2 = 2.24$. The liquid velocity components at the inlet orifices were assumed equal to zero.

The motion of the self-inducing turbine and its interaction with the stationary baffles was modelled with the Multiple Reference Frame (MRF) methodology. In the MRF method, the equations are expressed in a reference frame that rotates with the impeller speed and solved in steady state [34]. This method is often used since it is less time demanding than Sliding Mesh (SM) method, keeping accuracy and giving satisfactory results. Previous works have shown that the difference between the ensemble-averaged flow field calculated with the stationary and time dependent approaches was negligible [46,47]. The moving zone in the MRF approach was defined as a cylinder surrounding the impeller and the shaft, along the rotation

axis, with twice the height of the impeller blades. The cylinder radius is equidistant from blades tips and baffles.

The flow-governing conservation equations were solved with the finite-volume commercial CFD solver ANSYS Fluent 15. The Coupled pressure-based solver with a pseudo-transient algorithm available in Fluent was chosen for the coupling of the continuity and momentum conservation equations. The use of a pseudo-transient algorithm adds an unsteady term to the flow equations and has been reported to improve stability and the convergence behaviour of the solution [34]. The convective terms of the flow equations were discretized with a second order scheme and the mass conservation equations with a first order scheme. The turbulent kinetic energy of the liquid phase was initialized with a value equal to $k_L = 0.1\ \mathrm{m^2 s^{-2}}$ and the turbulence energy dissipation rate in the gas phase with a value equal to $\varepsilon_L = 10\ \mathrm{m^2 s^{-3}}$. All other variables like the velocities of both phases, the vessel pressure and the gas volume fraction were initialized with a value equal to zero. Steady-state solutions were achieved applying a pseudo-transient formulation and were accepted as converged for residuals smaller than 10^{-3}, ensuring as well the convergence of several monitored variables: gas hold up, dissipated power calculated from volume integration of turbulent dissipation rate, and the volume-averaged value of $k_L a$. The fluids used in the simulations were methylcyclohexane ($\rho_L = 770\ \mathrm{kg \cdot m^{-3}}$ and $\mu_L = 7.32 \times 10^{-4}\ \mathrm{Pa \cdot s}$) as the continuous phase and hydrogen as the dispersed phase ($\rho_G = 8.22 \times 10^{-1}\ \mathrm{kg \cdot m^{-3}}$ and $\mu_G = 8.83 \times 10^{-6}\ \mathrm{Pa \cdot s}$). Both fluids were considered to be incompressible.

4 Results and discussion

4.1 Multiphase flow simulation

The gas dispersion in the stirred tank was modelled using different correlations to take into account the apparent increase of drag due to the liquid phase turbulence generated by the impeller: the Brucato correlation [37], the Modified Brucato correlation [39] and the Pinelli correlation [40]. An analysis of the gas volume fraction distribution obtained from the simulations has been performed in order to choose the most suitable drag model (Figure 5). Assuming no drag modification due to turbulence effects, i.e. using the standard Schiller-Naumann correlation, the CFD simulations predict a high concentration of gas around the stirrer, mainly between the blades and disks, and in the top region of the reactor. No presence of gas is predicted in the bottom region of the reactor. Analyzing the experimental observations of the gas distribution in the reactor for the same stirring velocity of 1600 rpm on Figure 6, it is observed an accumulation of gas in the bottom region of the reactor. This indicates that the use of the standard Schiller-Naumann correlation for spheres in a quiescent liquid does not seem suitable to describe accurately the gas distribution in the reactor. In the case of the Brucato correlation, higher gas concentrations are predicted bellow the impeller, mainly in the axis of the stirrer. This result does not seem physically grounded, and it is not in agreement with the flow visualizations that show higher gas density at the top part of the reactor and not at the bottom (Figure 6). For this reason, the Brucato correlation has been excluded as well from further studies.

The Pinelli and Modified Brucato correlations seem to be the most suitable correlations to simulate the bench-scale reactor. Figure 6 shows the modelled and experimental gas distribution in the reactor at different stirring rates. Comparing the experimental visualizations and the CFD simulations, the Pinelli correction correlation seems, nonetheless, by qualitative comparison to overestimate as well the gas dispersion in the bottom part of the reactor.

Further discussion and explanation of the results obtained for the different drag modification correlations would require a deeper and more detailed study, which was considered to be out of the scope of this work. The authors were mostly focused here on the selection of the best correlation available to describe the impact of mechanically generated turbulence on the prediction of the gas distribution and $k_L a$ on the agitated vessel.

4.2 Mass transfer rate estimation

Volume averaged gas-liquid mass transfer coefficients, $\langle k_L a \rangle$, predicted with the CFD model were compared with results reported by Braga [24]. Braga [24] investigated experimentally the gas/liquid mass transfer in a bench-scale reactor very similar to the simulated geometry in this work: a cylindrical, flat-bottomed reactor equipped with a double-disc hollow self-inducing impeller, resembling to a Ruston turbine with a diameter of 19 mm. The only difference between the simulated reactor and Braga's [24] reactor is their diameter: the reactor of Braga has a diameter of 62 mm against the 58 mm assumed the simulation's geometry. In the simulations and experiments the same gas (hydrogen) and liquid (methylcyclohexane) were considered. The reactor was filled until the same liquid height (50 mm). The experimental methodology followed by Braga [24] to determine $\langle k_L a \rangle$ coefficients was the method of physical absorption. This method has been described previously by several authors [2,19,20] and consists on measuring the total pressure variation in the agitated reactor during batch operation.

Figure 7 shows the contour maps of simulated local $k_L a$ values in a vertical plane in the reactor, passing through the impeller axis, for the different impeller rotational velocities, and assuming a spatially invariant bubble diameter of 2 mm, based on experimental validations, and using the modified Brucato and Pinelli drag coefficient corrections. The CFD results on Figure 7 show that the mass transfer rate between the two phases is not spatially uniform in

the reactor, varying by at least 4 orders of magnitude in the domain. As expected, local $k_L a$ values are higher in the region closer to the impeller where both gas-liquid interfacial area and turbulent energy dissipation rate are higher. The results on Figure 7 also show that in the range from 1000 to 2000 rpm, the values of $k_L a$ can increase considerably inside de vessel, by at least one order of magnitude, with the increase of N. This is due simultaneously to the increase of the gas induction rate into the system and to the increase of turbulent energy dissipation in the domain with the increase of the impeller rotational velocity.

The numerical predictions of local values of $k_L a$ were volume-averaged to be compared with the experimental measurements of mean mass transport rates from Braga results [24]. The volume average value of the $k_L a$ was calculated as

$$\langle k_L a \rangle = \frac{1}{V_{\text{reactor}}} \iiint_{V_{\text{reactor}}} k_L(\vec{x}) a(\vec{x}) \, \mathrm{d}^3\vec{x} \tag{20}$$

where $\vec{x}$ is the position vector inside the reactor volume V_{reactor}. The comparison of these two values is only possible by considering the same assumptions adopted in the experimental work of [24]: the characteristic time for mixing is much lower than the characteristic time for mass exchange between the gas and the liquid phases, i.e., the concentration of hydrogen in the liquid phase can be considered homogeneous in the stirred tank. While showing a similar trend and predicting values in the same order of magnitude, the CFD simulations using the Pinelli modification correlation tend to overestimate the values of $\langle k_L a \rangle$ (Figure 8). CFD simulations using the Modified Brucato correction seem to be more consistent with experimental data. The deviation between CFD results and experimentation can be due to the approximation of a constant and spatially homogeneous bubble size and shape. An experimental characterization of the bubble size distribution, breakup and coalescence inside

the reactor must be performed in order to refine the model and, in turn, matching even further the computational predictions of $\langle k_L a \rangle$ with the results of Braga [24]

The experimental results and CFD simulations using the Modified Brucato correlation where compared as well with values predicted by the correlation proposed by [2] (Figure 9), which is the correlation most frequently used in the characterization of interfacial mass transfer of small-scale stirred reactors with self-inducing impellers:

$$\mathrm{Sh}_{G/L} = B\,\mathrm{Re}_{\mathrm{imp}}^{1.45}\,\mathrm{We}_{\mathrm{imp}}^{0.5}\,\mathrm{Sc}^{0.5} \tag{21}$$

where $\mathrm{Sh}_{G/L} = k_L a D^2 / D_m$ is the Sherwood number, $\mathrm{Re}_{\mathrm{imp}} = ND^2\rho_L / \mu_L$ the impeller Reynolds number, $\mathrm{We}_{\mathrm{imp}} = N^2 D^3 \rho_L / \sigma$ the Weber number based on the impeller dimensions and speed, $\mathrm{Sc} = \mu_L / (\rho_L D_m)$ the Schmidt number, and D the impeller diameter. The constant B is given by

$$B = \begin{cases} 3\times10^{-4} & \text{if } H/T = 1 \\ 1.5\times10^{-4} & \text{if } H/T = 1.4 \end{cases} \tag{22}$$

depending on the ratio between the height of the liquid in the vessel, H, and its diameter, T. Figure 9 shows that the Dietrich correlation [2] overestimates $\langle k_L a \rangle$ values. In the bench-scale reactor used in this study, the developed model is more accurate in the estimation of mass transfer rates.

5 Conclusions

A CFD Eulerian-Eulerian model of the gas-liquid flow in a bench-scale stirred tank reactor equipped with a self-inducing impeller has been developed. Danckwerts' bubble surface renewal model was coupled to multiphase CFD simulations for the prediction of mass transfer rate coefficients at different impeller speeds. Different drag modification laws proposed in the

literature to take into account the effect of mechanically generated turbulence on the rising velosities of the gas bubbles were considered in this study.

From this study, a selection of suitable modelling parameters and correlations has been proposed. While being based on some simplifications, the proposed CFD methodology is able to predict interphase mass transfer rate values with more accuracy when compared with the most frequent correlation used in the industrial practice for characterisation mass transfer on small-scale stirred tank reactors with self-inducing gas turbines. Efforts have been made develop a computationally inexpensive modelling methodology in order to offer an attractive optimisation tool for multiphase lab scale reactors. With the proposed CFD methodology, the estimated values of $\langle k_L a \rangle$ show good agreement with experimental observations reported in the literature. The results of this work illustrate the relevance and usefulness of using advanced modelling techniques in the study and design of multiphase chemical reactors, especially when these devices are in a dimension range or have a design for which only few studies exist in the literature. Additionally, this study shows that further research on the impact of mechanically generated turbulence on the rising/settling velocities of droplets, bubbles or solid for the simulation of multiphase turbulent flows is still required.

6 Symbols and Nomenclature

a	[m^{-1}]	Specific surface area
a_1		Constant
a_2		Constant
b_1		Constant
b_2		Constant
b_3		Constant
C_D		Drag coefficient
$\overline{C_D}$		Modified drag coefficient
CFD		Computational Fluid Dynamics
d_b	[m]	Bubble diameter
d_o	[m]	Orifice diameter
D_m	[$m^2 s^{-1}$]	Molecular diffusion coefficient

Eo		Eötvös number
F_{Drag}	[kg m^{-2} s^{-2}]	Volumetric drag forces
$F_{Non-Drag}$	[kg m^{-2} s^{-2}]	Volumetric non-drag forces
g	[m s^{-2}]	Gravity acceleration
$\bar{\bar{I}}$		Identity tensor
k	[m^{2}s^{-2}]	Turbulent kinetic energy
k_L	[s^{-1}.m]	Gas/liquid mass transfer
$k_L a$	[s^{-1}]	Gas/liquid mass transfer
N	[rps]	Impeller speed
PBM		Population Balance Models
Q_G	[m^{3}s^{-1}]	Induced gas flow rate
Re		Particle relative Reynolds number
s	[s^{-1}]	Fractional rate of surface-element replacement
$Sc_{t,VOF}$		Schmidt VOF turbulent number
α_G		Gas volume fraction
α_L		Liquid volume fraction
ε	[m^{2}s^{-3}]	Average turbulent dissipation rate
ε_L	[m^{2}s^{-3}]	Average liquid turbulent dissipation rate
ρ_L	[kg m^{-3}]	Liquid density
v_L	[m s^{-1}]	Liquid velocity
∇p	[N m^{-2}]	Pressure Loss
$\bar{\bar{\tau}}_L$	[kg m^{-1} s^{-2}]	Liquid phase stress tensor
Γ	[m^{2}s^{-1}]	VOF turbulent dispersion coefficient
$\nu_{t,L}$	[m^{2}s^{-1}]	Kinematic liquid turbulent eddy viscosity
ν_L	[m^{2}s^{-1}]	Liquid dynamic viscosity
μ_L	[kg m^{-1}s^{-1}]	Liquid shear viscosity
λ_K	[m^{-1}]	Kolomogrov length scale
λ_L	[kg m^{-1}s^{-1}]	Liquid bulk viscosity
Δp_{imp}	[Pa]	Pressure drop due to friction
σ	[Nm^{-1}]	Superficial tension
CFD		Computational Fluid Dynamics
PBM		Population Balance Models

7 References

[1] P. Danckwerts, Significance of liquid-film coefficients in gas absorption, Ind. Eng. Chem 43 (1951) 1460–1467.

[2] E. Dietrich, C. Mathieu, H. Delmas, J. Jenck, Raney-nickel catalyzed hydrogenations: Gas-liquid mass transfer in gas-induced stirred slurry reactors, Chemical Engineering Science 47 (1992) 3597–3604.

[3] G.Q. Martin, Gas-inducing agitator, Ind. Eng. Chem. Process Des. Develop. 11 (1972) 397–404.

[4] N.A. Deshmukh, S.S. Patil, J.B. Joshi, Gas Induction Characteristics of Hollow Self-Inducing Impeller, Chemical Engineering Research and Design 84 (2006) 124–132.

[5] J.B. Joshi, Sharma, M. M., Mass transfer and hydrodynamic characteristics of gas inducing type of agitated contactors, The Canadian Journal of Chemical Engineering 55 (1977) 683–695.

[6] S.B. Sawant, J.B. Joshi, Critical impeller speed for the onset of gas induction in gas-inducing types of agitated contactors, An International Journal of Research and Development 18 (1979) 87–91.

[7] J.B. Joshi, Modifications in the Design of Gas Inducing Impeller, Chemical Engineering Communications 5 (1980) 109–114.

[8] K. Saravanan, V.D. Mundale, J.B. Joshi, Gas Inducing Type Mechanically Agitated Contactors, Ind. Eng. Chem. Res. 33 (1994) 2226–2241.

[9] K. Saravanan, V.D. Mundale, A.W. Patwardhan, J.B. Joshi, Power consumption in gas-inducing-type mechanically agitated contactors, Ind. Eng. Chem. Res. 35 (1996) 1583–1602.

[10] S.E. Forrester, C.D. Rielly, K.J. Carpenter, Gas-inducing impeller design and performance characteristics, Chem. Eng. Sci 53 (1998) 603–615.

[11] A.W. Patwardhan, J.B. Joshi, Design of Gas-Inducing Reactors, Ind. Eng. Chem. Res. 38 (1999) 49–80.

[12] Zieverink, M. M. P., M.T. Kreutzer, F. Kapteijn, J. Moulijn, Gas-liquid mass transfert in benchscale stirred tanks- fluid properties and critical impeller speed for gas induction, Ind. Eng. Chem. Res. 45 (2006) 4574–4581.

[13] B.N. Murthy, N.A. Deshmukh, A.W. Patwardhan, J.B. Joshi, Hollow self-inducing impellers: Flow visualization and CFD simulation, Chem. Eng. Sci 62 (2007) 3839–3848.

[14] B.N. Murthy, R.S. Ghadge, J.B. Joshi, CFD simulations of gas-liquid-solid stirred reactor: prediction of critical impeller speed for solid suspension, Chem. Eng. Sci 62 (2007) 7184–7195.

[15] B.N. Murthy, R.B. Kasundra, J.B. Joshi, Hollow self-inducing impellers for gas-liquid-solid dispersion: Experimental and computational study, Chem. Eng. J. 141 (2008) 332–345.

[16] E.H. Stitt, Alternative multiphase reactors for fine chemicals: A world beyond stirred tanks?, Chem. Eng. J. 90 (2002) 47–60.

[17] G. Ascanio, B. Castro, E. Galindo, Measurement of Power Consumption in Stirred Vessels—A Review, Chemical Engineering Research and Design 82 (2004) 1282–1290.

[18] A. Deimling, B.M. Karandikar, Y.T. Shah, N.L. Carr, Solubility and mass transfer of CO and H2 in Fischer—Tropsch liquids and slurries, The Chemical Engineering Journal 29 (1984) 127–140.

[19] R.V. Chaudhari, R.V. Gholap, G. Emig, H. Hofmann, Gas-liquid mass transfer in "dead-end" autoclave reactors, The Canadian Journal of Chemical Engineering 65 (1987) 744–751.

[20] V. Meille, N. Pestre, P. Fongarland, C. de Bellefon, Gas/liquid mass transfer in small laboratory batch reactors: Comparison of methods., Industrial & Engineering Chemistry Research 43 (2004) 924–927.

[21] M. Mitrovic, Étude des transferts de matière dans un réacteur triphasique gaz-liquide-solide, d'investigation cinétique (réacteur Robinson-Mahoney), Université Claude Bernard Lyon 1, France (2001).

[22] K.C. Ruthiya, van der Schaaf, J, Kuster, B. F. M, J.C. Schouten, Mechanisms of physical and reaction enhancement of mass transfer in a gas inducing stirred slurry reactor, Chemical Engineering Journal 96 (2003) 55–69.

[23] I. Pitault, P. Fongarland, D. Koepke, M. Mitrovic, D. Ronze, M. Forissier, Gas–liquid and liquid–solid mass transfers in two types of stationary catalytic basket laboratory reactor, Chemical Engineering Science 60 (2005) 6240–6253.

[24] M. Braga, Etude des phénomènes de transfert et de l'hydrodynamique dans des réacteurs agités à panier catalytique, PhD Thesis, Université Claude Bernard Lyon 1, Lyon, France, 2013.

[25] A. Buffo, M. Vanni, D.L. Marchisio, Multidimensional population balance model for the simulation of turbulent gas–liquid systems in stirred tank reactors, 4th International Conference on Population Balance Modeling 70 (2012) 31–44.

[26] J. Gimbun, C.D. Rielly, Z.K. Nagy, Modelling of mass transfer in gas–liquid stirred tanks agitated by Rushton turbine and CD-6 impeller: A scale-up study, Chemical Engineering Research and Design 87 (2009) 437–451.

[27] K.E. Morud, B.H. Hjertager, LDA measurements and CFD modelling of gas-liquid flow in a stirred vessel, Chemical Engineering Science 51 (1996) 233–249.

[28] A.R. Khopkar, V.V. Ranade, CFD simulation of gas–liquid stirred vessel: VC, S33, and L33 flow regimes, AIChE J. 52 (2006) 1654–1672.

[29] H. Sun, Z.-S. Mao, G. Yu, Experimental and numerical study of gas hold-up in surface aerated stirred tanks, Chemical Engineering Science 61 (2006) 4098–4110.

[30] Wang, Z.-S. Mao, C. Yang, Experimental and Numerical Investigation on Gas Holdup and Flooding in an Aerated Stirred Tank with Rushton Impeller, Industrial & Engineering Chemistry Research 45 (2006) 1141–1151.

[31] F. Scargiali, A. D'Orazio, F. Grisafi, A. Brucato, Modelling and Simulation of Gas–Liquid Hydrodynamics in Mechanically Stirred Tanks, Chem. Eng. Res. Des. 85 (2007) 637–646.

[32] M. Jahoda, L. Tomášková, M. Moštěk, CFD prediction of liquid homogenisation in a gas–liquid stirred tank, 13th European Conference on Mixing: New developments towards more efficient and sustainable operations 87 (2009) 460–467.

[33] A. Sokolichin, G. Eigenberger, A. Lapin, Simulation of buoyancy driven bubbly flow: Established simplifications and open questions, AIChE J. 50 (2004) 24–45.

[34] ANSYS, ANSYS FLUENT Theory Guide- Release 15.0.

[35] L. Schiller and Z. Naumann, "A drag coefficient correlation", Z. Ver. Deutsch. Ing. 77 (1935).

[36] T. Takamasa and A. Tomiyama, Three-Dimensional Gas-Liquid Two-Phase Bubbly Flow in a C-Shaped Tube, Ninth International Topical Meeting on Nuclear Reactor Thermal Hydraulics (NURETH-9), San Francisco, CA, 1998.

[37] A. Brucato, F. Grisafi, G. Montante, Particle drag coefficients in turbulent fluids, Chem. Eng. Sci 53 (1998) 3295–3314.

[38] E. Doroodchi, G.M. Evans, M.P. Schwarz, G.L. Lane, N. Shah, A. Nguyen, Influence of turbulence intensity on particle drag coefficients, Chemical Engineering Journal 135 (2008) 129–134.

[39] G. Lane, M.P. Schwarz, G.M. Evans, Chapter 25 – Modelling of the Interaction between Gas and Liquid in Stirred Vessels, 10th European Conference on Mixing Proceedings of the 10th European Conference, Delft, The Netherlands, July 2–5 (2000).

[40] D. Pinelli, M. Nocentini, F. Magelli, Solids distribution in stirred slurry reactors: Influence of some mixer configurations and limits to the applicability of a simple model for predictions, Chem. Eng. Comm. 188 (2001) 91–107.

[41] J.C. Lamont, D.S. Scott, An eddy cell model of mass transfer into the surface of a turbulent liquid., AIChE J. 16 (1970) 513–519.

[42] C.R. Wilke, P. Chang, Correlation of diffusion coefficients in dilute solutions., AIChE J. (1955) 264–270.

[43] M. Coroneo, G. Montante, A. Paglianti, F. Magelli, CFD prediction of fluid flow and mixing in stirred tanks: Numerical issues about the RANS simulations, Comput. Chem. Eng. 35 (2011) 1959–1968.

[44] D. Zhang, N.G. Deen, J. Kuipers, Numerical simulation of the dynamic flow behavior in a bubble column: A study of closures for turbulence and interface forces, Chem. Eng. Sci 61 (2006) 7593–7608.

[45] C. P. Fonte, B. S. Pinho, V. Santos-Moreau, B. Lopes, José Carlos, Prediction of the induced gas flow rate from a self-inducing impeller with CFD, Chem. Eng. Technol. 37 (2014) 571–579.

[46] G. Montante, K.C. Lee, A. Brucato, M. Yianneskis, Numerical simulations of the dependency of flow pattern on impeller clearance in stirred vessels, Chem. Eng. Sci 56 (2001) 3751–3770.

[47] J. Aubin, D.F. Fletcher, C. Xuereb, Modeling turbulent flow in stirred with CFD: the influence of the modeling approach, turbulencemodel and numerical scheme, Exp. Therm. Fluid Sci. 28 (2004) 431–445.

List of Figures

Figure 6. Simulated and experimental gas distribution in the reactor at different stirring rates. Simulation using Modified Brucato and Pinelli correlations.

Figure 7. Contours of local $k_L a$ values in a vertical plane of the reactor passing through the axis for a constant bubble diameter of 2 mm and different impeller rotational speeds using modified Brucato and Pinelli correlations.

Figure 8. Volume-average value of $k_L a$ as a function of the impeller rotational speed determined experimentally by [24,24] and from the CFD simulations for a bubble diameter of 2 mm using Brucato Modified and Pinelli models.

Figure 9. Volume-average value of $k_L a$ as a function of the impeller rotational speed determined experimentally by [24,24], from CFD simulations for a bubble mean diameter of 2 mm using Brucato Modified model and using Dietrich correlation.

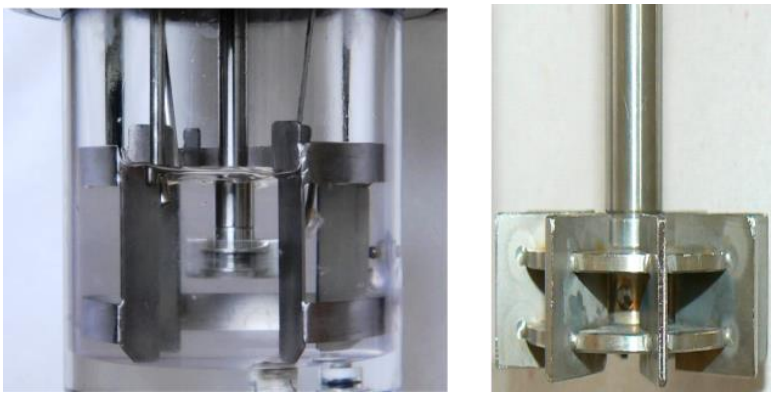

Figure 1. Transparent reactor (left) and self-inducing impeller (right).

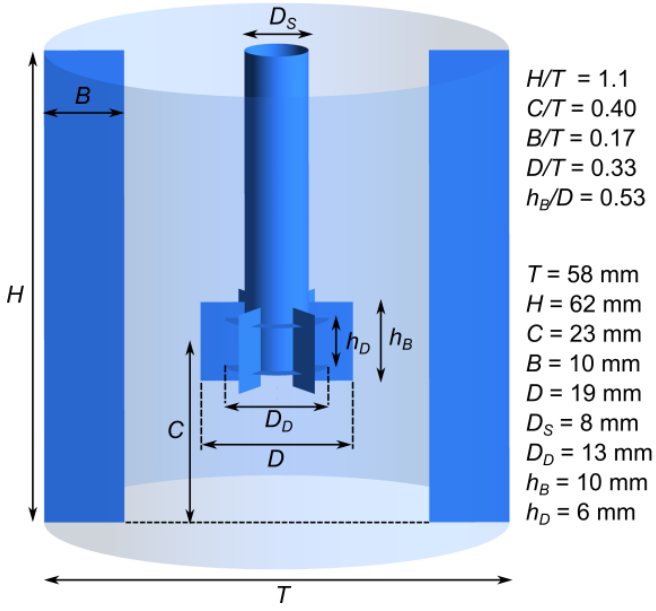

Figure 2. Schematic representation and dimensions of the simulated stirred tank reactor.

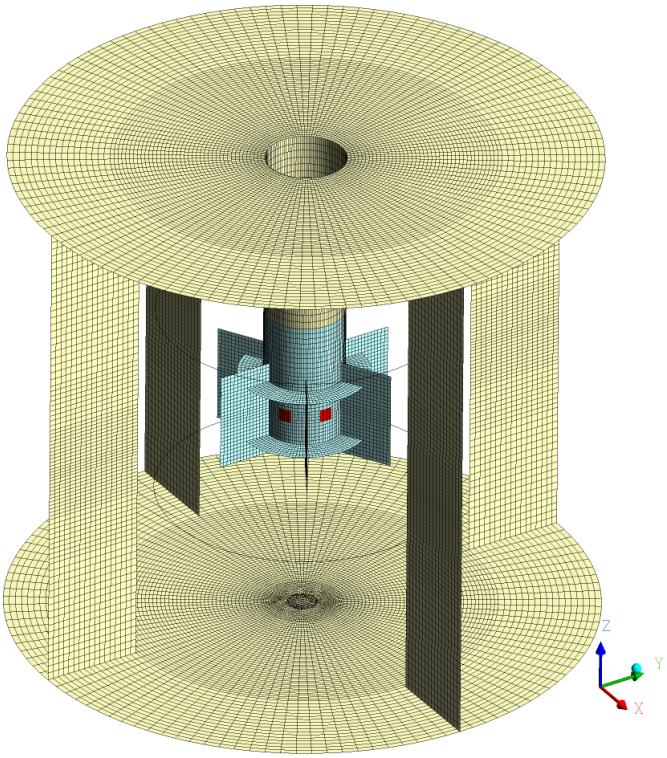

Figure 3. Mesh of the entire stirred tank.

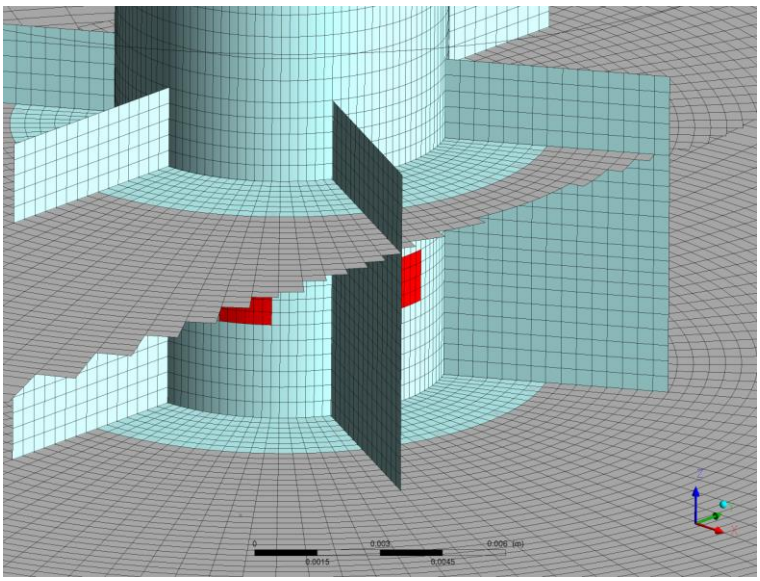

Figure 4. Detail of the mesh near the impeller.

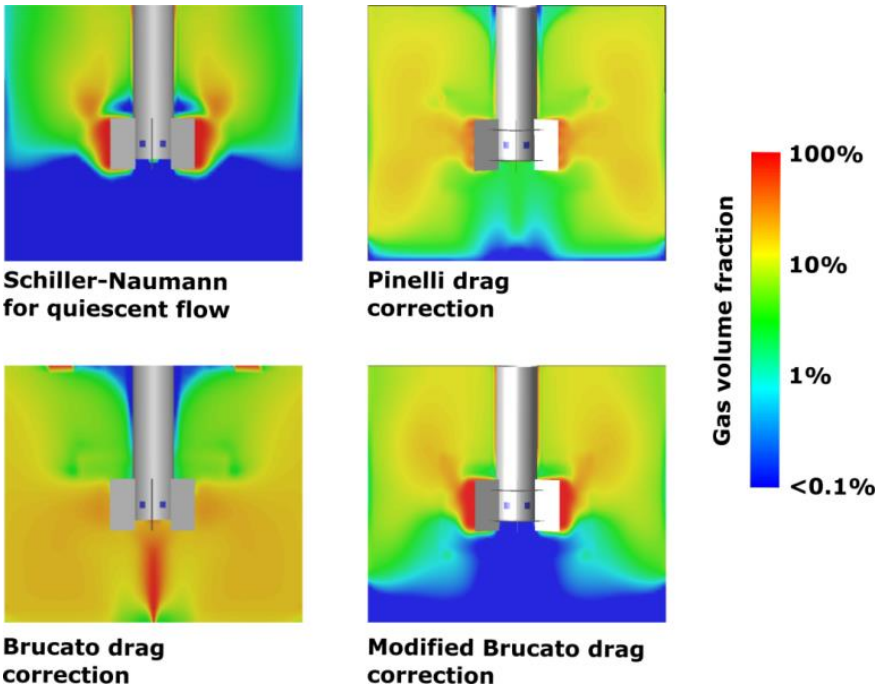

Figure 5. Gas volume fraction inside the reactor at 1600 rpm using no drag modification, and the Pinelli, Brucato and Modified Brucato corrections.

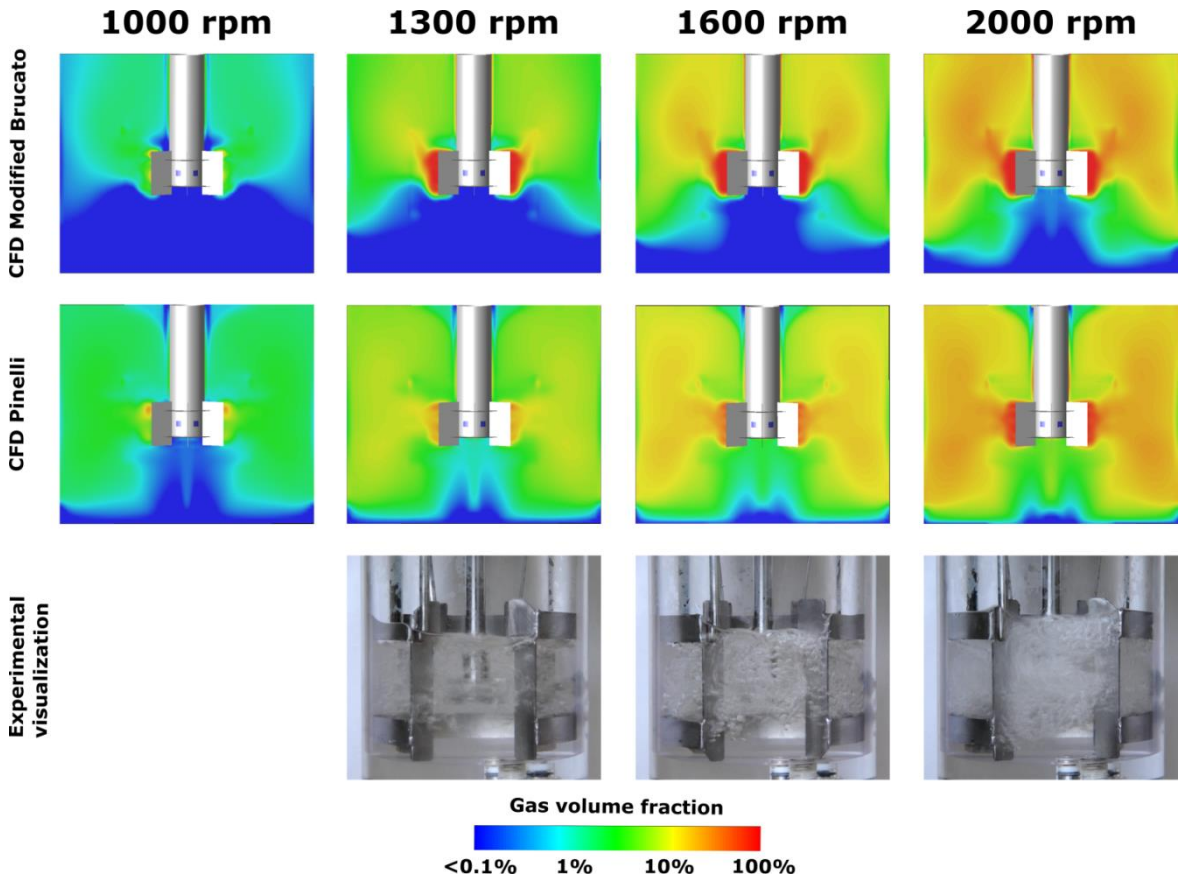

Figure 6. Simulated and experimental gas distribution in the reactor at different stirring rates. Simulation using Modified Brucato and Pinelli correlations.

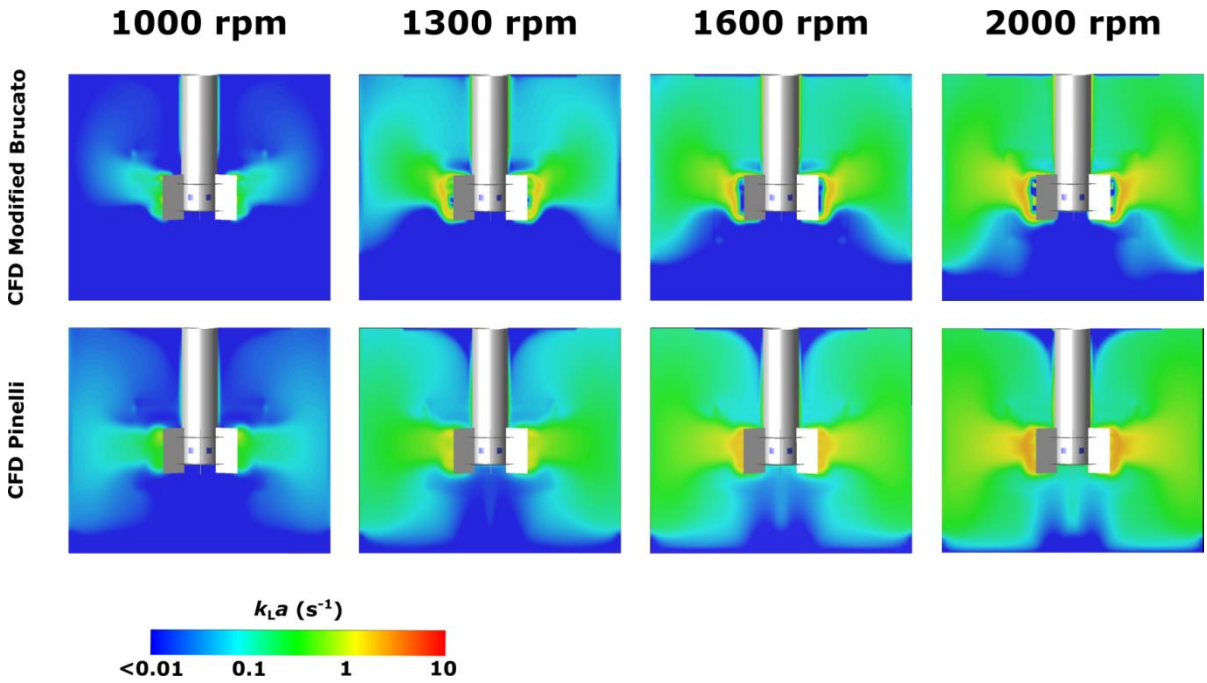

Figure 7. Contours of local k_La values in a vertical plane of the reactor passing through the axis for a constant bubble diameter of 2 mm and different impeller rotational speeds using modified Brucato and Pinelli correlations.

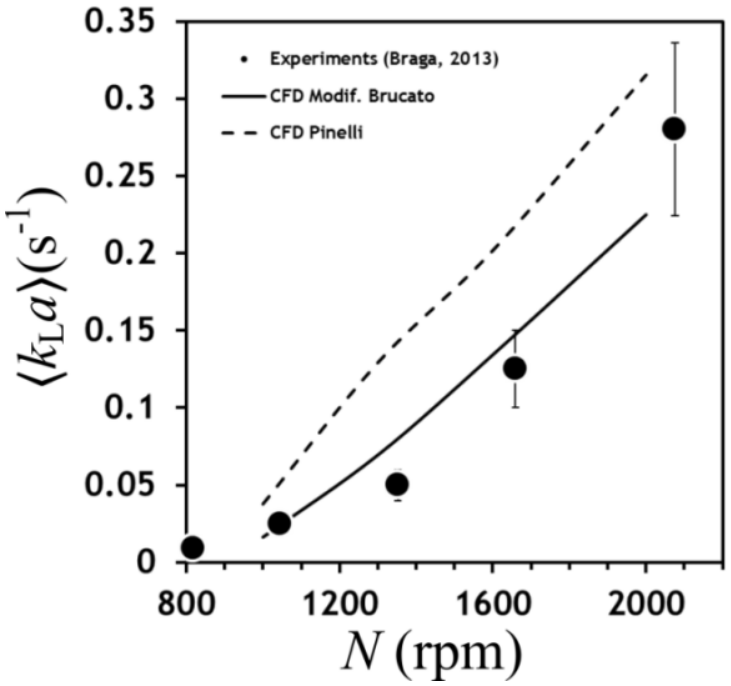

Figure 8. Volume-average value of $k_L a$ as a function of the impeller rotational speed determined experimentally by [24,24] and from the CFD simulations for a bubble diameter of 2 mm using Brucato Modified and Pinelli models.

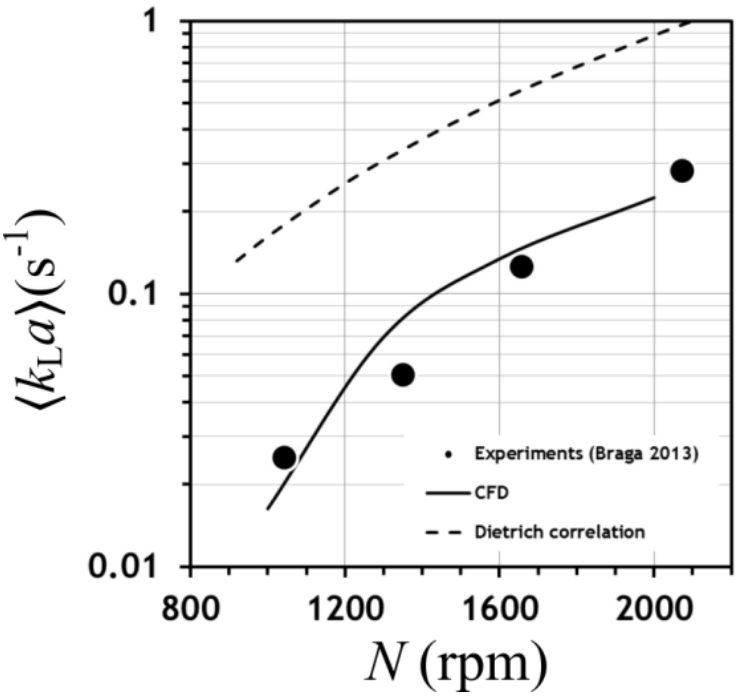

Figure 9. Volume-average value of $k_L a$ as a function of the impeller rotational speed determined experimentally by [24,24], from CFD simulations for a bubble mean diameter of 2 mm using Brucato Modified model and using Dietrich correlation.